A Compact Wideband Dual-Polarized Antenna With Enhanced Upper Out-of-Band Suppression

Le-Hu Wen, Steven Gao, *Fellow, IEEE*, Qi Luo, *Member, IEEE*, Qingling Yang, Wei Hu, *Member, IEEE* and Yingzeng Yin, *Member, IEEE*, Xiaofei Ren, Jian Wu

***Abstract*—A compact wideband dual-polarized antenna with enhanced upper out-of-band suppression is presented in this paper. The proposed antenna is equivalent as two electric dipoles and two magnetic dipoles by using the crossed shunt loops. The incorporation of the electric and magnetic dipoles makes the antenna achieve wide impedance bandwidth and compact radiator size. In addition, four parasitic strips are inserted near the inner edge of the four loops to enhance the antenna upper out-of-band suppression at 3.5 GHz with improved impedance bandwidth. The antenna is fed by the crossed coaxial baluns with high isolation. A shorting sheet is introduced into the baluns to further enhance the upper out-of-band suppression and create another rejection at 4.9 GHz. To demonstrate the design method, the proposed antenna prototype was fabricated and measured. Measured results show that the proposed antenna has a wide impedance bandwidth of 1.625-3.05 GHz (61%) for S_{11}<-14 dB with the isolation better than 38.3 dB. The upper out-of-band suppression of the antenna is also largely enhanced with measured S_{11}>-2 dB from 3.35 GHz to 5.25 GHz. In addition, stable antenna gain and radiation patterns are achieved for base station applications.**

***Index Terms*—Balun, dual-polarized antenna, electric dipole, magnetic dipole.**

I. Introduction

Owing to advantages of combating the multi-path fading effect and increasing the channel capacity to the wireless communication systems, dual-polarized antennas have received much popularity in different application scenarios, such as base stations, satellites, and radars systems. However, as the development of these communication systems, many challenges are needed to be resolved, including the increased communication bandwidth, the increasingly limited antenna installation space, and the undesired interferences from other wireless communication systems [1]-[2].

Patch antennas are a popular type of radiators to realize dual-polarization with low profile configuration [3]-[10]. To increase the antenna impedance bandwidth and achieve high port isolation, slot coupling and aperture coupling [3]-[7] are the commonly used methods with the multi-layer configuration.

This work was supported in part by China Research Institute of Radiowave Propagation, in part by EPSRC grants EP/N032497/1 and EP/P015840/1, and in part by scholarship from the China Scholarship Council. *(Corresponding author: Le-Hu Wen)*

L.-H. Wen, S. Gao, Q. Luo, and Q. Yang are with the School of Engineering and Digital Arts, University of Kent, Canterbury CT2 7NT, U.K. (e-mail: lw347@kent.ac.uk)

W. Hu and Y. Yin are with the National Key Laboratory of Antennas and Microwave Technology, Xidian University, Xian 710071, China.

X. Ren and J. Wu are with the Innovation and Research Center, China Research Institute of Radiowave Propagation, Qingdao, 266107, China.

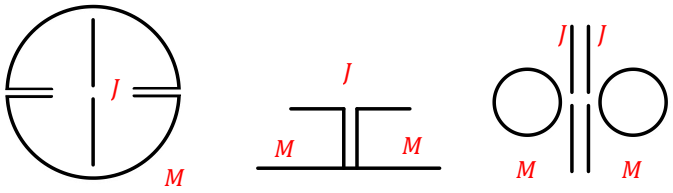

(a) (b) (c)

Fig. 1. Equivalent electric dipole and magnetic dipole configurations. (a) Reference [20]. (b) Reference [23]. (c) Proposed antenna.

In [8], the hybrid feed method is applied to realize dual-polarization with high port isolation of 43 dB and low cross-polarization level of -37 dB. In [9]-[10], novel resonator feed methods are utilized to realize wideband and dual-band dual-polarized antennas. However, patch antennas of these kinds are usually facing the problems of narrow bandwidth due to the low-profile configuration. Although the bandwidths of these patch antennas fed by the multi-mode resonators are enlarged, the radiation patterns are also affected by the parasitic radiation from the loaded slots and resonators.

Compared to the other communication systems, base stations require a much wider range of bandwidth for wireless mobile communication, which usually need to cover the bandwidth of 1.7-2.7 GHz for 2G/3G/4G requirements. To obtain a broad bandwidth, various dual-polarized crossed dipole antennas are reported in recent years [11-19]. In [12] and [13], fan-shaped dipoles and bowtie-shaped dipoles are proposed with wide bandwidth and high isolation. In [14]-[16], different parasitic elements are used to improve the antenna bandwidth and stabilize the radiation patterns. Also, printed integrated baluns [17]-[18] and tuned loop [19] are introduced to design dual-polarized antennas. These dual-polarized antennas can normally meet the current requirements for base stations. However, with the development of base station systems [26], 5G frequency bands have already been licensed in China. Two sub-6G frequency bands, which are 3.4-3.6 GHz and 4.8-5 GHz, could have produced interferences to the current 2G/3G/4G base station systems. In addition, the newly introduced 5G antennas will lead to the more limited space for base station antennas. So it is necessary to develop compact antennas with high suppression at the 5G bands for the current 2G/3G/4G base stations.

Recently, metamaterial-inspired, near-field resonant parasitic, Huygens source antennas are reported to realize electrically small antennas [20]-[22]. By using near-field resonant parasitic elements, both electric and magnetic dipoles are integrated to achieve Huygens source radiation with very

compact configurations. However, the bandwidth of these proposed antennas is normally not wide enough to cover base station requirement, and these antennas are mainly focused on the single-polarized antennas or circularly polarized antennas. Dual-polarized magneto-electric dipole antennas in [23]-[25] have achieved wide impedance bandwidth, but large spaces are occupied compared to the Huygens source antennas.

In this paper, a novel dual-polarized antenna with electric and magnetic resonances is proposed with wide impedance bandwidth and compact radiator size. Fig. 1 compares the proposed equivalent electric dipole and magnetic dipole configuration with the Huygens source antenna [20] and the magneto-electric dipole antenna [23]. Huygens source antennas feature electrically small configuration owing to the incorporation of both an electric dipole and a magnetic dipole. Magneto-electric dipole antennas are a combination of resonating dipole mode and patch mode. The equivalent electric dipole and magnetic dipole configuration for our proposed antenna is shown in Fig. 1(c), which is different from these two types, and composed of two electric dipoles and two magnetic dipoles. The proposed antenna can also be seen as a new type of the printed biquad antennas [27]-[30]. However, the traditional biquad antennas are normally realized for single-polarization, and radiate as the electric dipoles.

The equivalent electric dipoles and magnetic dipoles are developed by the crossed shunt loops, which make the proposed antenna achieve wider impedance bandwidth and more compact size. Compared to the first matching frequency of the single-polarized shunt loop antenna, the first matching frequency of the dual-polarized crossed shunt loop antenna is only 1/3 of its counterpart. This means large antenna size can be reduced owing to the introduction of electric dipoles and magnetic dipoles. Furthermore, four parasitic strips are introduced near the inner edge of the loops, which not only help to enlarge the antenna impedance bandwidth, but also improve the antenna selectivity and produce the first suppression at 3.5 GHz. In addition, crossed coaxial baluns are used to feed the proposed antenna with the newly introduced shorting sheet, which is utilized to create the second suppression at 4.9 GHz. Therefore, two radiation nulls are achieved at the center of two 5G base stations bands.

To validate the design concept, the proposed dual-polarized antenna is designed, fabricated, and measured. The measured results show that the proposed antenna has a wide impedance bandwidth of 1.625-3.05 GHz (61%) for S_{11}<-14 dB and high isolation of 38.3 dB with a compact radiator size. Furthermore, enhanced upper out-of-band suppression from 3.35 GHz to 5.25 GHz with S_{11}>-2 dB is achieved with two radiation nulls at the desired frequency of 3.5 GHz and 4.9 GHz. Stable antenna gain and beamwidth are also achieved for base station applications.

II. Dual-Polarized Antenna

A. Configuration

The configuration of the proposed dual-polarized antenna is shown in Fig. 2. This antenna is composed of a square antenna reflector, two crossed coaxial baluns, and the antenna radiator. The antenna is designed of ±45° polarizations for base station applications. The square reflector is made up of a square copper sheet with the length of 140 mm, which is designed for the unidirectional radiation and low back radiation. The antenna radiator is printed on both sides of a Rogers 4003C substrate with the dielectric constant of 3.55 and the thickness of 0.813

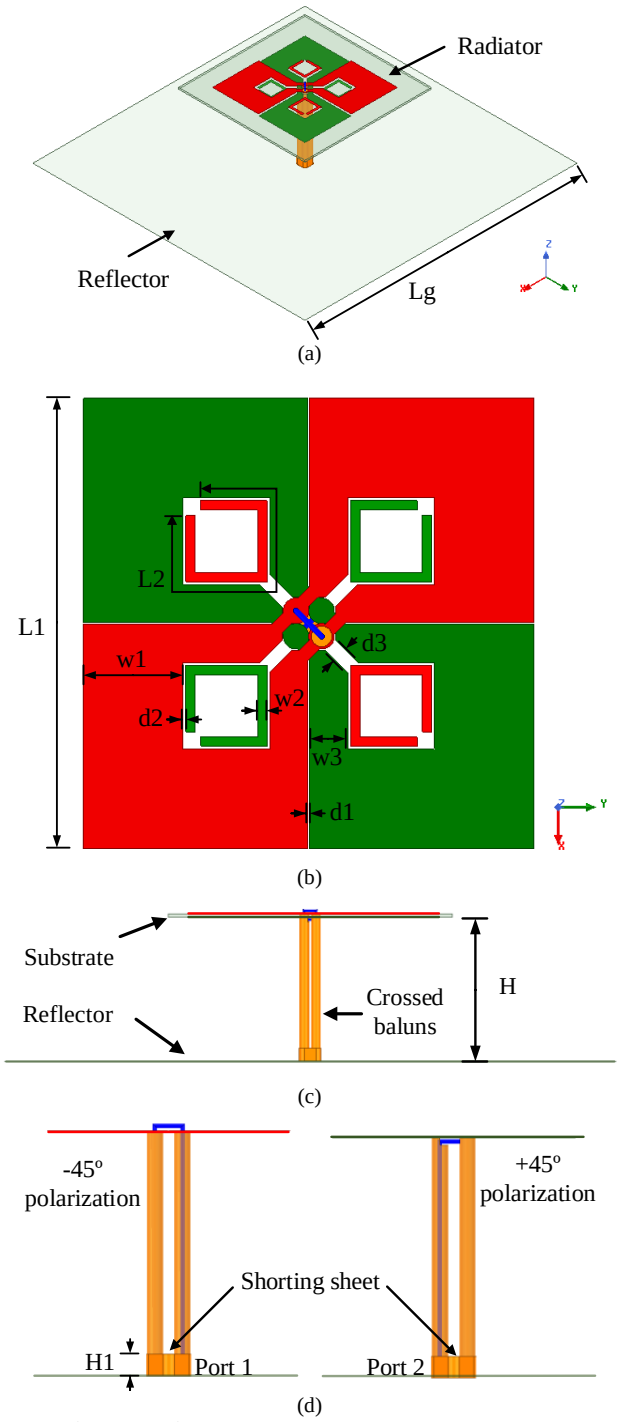

Fig. 2. Configuration of the proposed dual-polarized antenna. (a) 3D view. (b) Top view of the antenna radiator. (c) Side view. (d) Details of the crossed coaxial baluns. (Detailed parameters of the proposed dual-polarized antenna. Lg=140 mm, L1=47.5 mm, L2=27.5 mm, w1=10.5 mm, w2=1 mm, w3=4 mm, d1=0.2 mm, d2=0.3 mm, d3=1.5 mm, H=33 mm, H1=3 mm)

mm. Two crossed coaxial baluns are used to feed the top radiator with balanced excitation magnitude and phase, which are of great importance to improve the antenna isolation.

Fig. 2 (b) shows the detailed configuration of the antenna radiator. It consists of two pairs of crossed shunt loops. Note that one pair is printed on the top layer of the substrate, which is realized for -45º polarization. Another pair is printed on the bottom layer and realized for +45º polarization. These two pairs of shunt loops are of the same size and symmetrical to each other with the stepped line width of w1 and w3. The distance between the edges of two crossed loops is d1. These three parameters are important to the improvement of antenna input impedance. By using the crossed shunt loops, electric and magnetic resonance characteristic is introduced with the compact radiator size. Four parasitic strips are located near the inner edge of the loops, and they can further broaden the antenna impedance bandwidth and introduce the first suppression at 3.5 GHz. In the figure, the copper on the top layer of the substrate is depicted in red color, and the copper on the bottom layer is depicted in green color.

Fig. 2 (c) shows the side view of the dual-polarized antenna. The distance from the top radiator to the antenna reflector is designed as 33 mm to obtain stable unidirectional radiation for base station applications. To realize high port isolation, crossed coaxial baluns are used to feed the proposed dual-polarized antenna. The detailed side view of the crossed coaxial baluns is shown in Fig. 2 (d). For the -45º polarization, the outer conductors of the two coaxial cables are connected to both sides of the shunt loops, while the inner conductor of one coaxial cable is penetrated through one shunt arm, and connected to the other shunt arm on the top layer. For the +45º polarized shunt loops, the outer conductors of the coaxial cables are also soldered to the two center strips of loops, while the inner conductor of one cable is soldered to the outer conductor of the other cable. In addition, a shorting sheet is added at the end of the crossed baluns, which is used to introduce the second upper suppression at 4.9 GHz. All the simulation works in this paper are with the help of Ansys HFSS 18.0. The details of the optimized parameters for the dual-polarized antenna are shown in the caption of Fig. 2.

B. Equivalent Electric Dipoles and Magnetic Dipoles

The proposed antenna can be equivalent as a combination of electric dipoles and magnetic dipoles. Therefore, electric and magnetic resonances are developed by using the crossed shunt loops. Two simplified antenna models are used to illustrate the different resonance characteristics of electric and magnetic dipoles, and they are shown in Fig. 3. In this figure, Antenna 1 is the simplified antenna for dual-polarization by using crossed shunt loops, which is excited by the ideal lump ports. Antenna 2 is the single-polarized counterpart with only one shunt loops. Both two reference antennas are simulated with the same antenna reflectors, and the reflectors are also of the same size as the proposed antenna in Fig. 2.

Fig. 4 (a) shows the simulated S-parameters of the two reference antennas. The impedance bandwidth of Antenna 1 for S_{11}<-15 dB is from 1.65 GHz to 2.6 GHz, and two reflection zeroes are observed at 1.74 GHz and 2.36 GHz. Whereas the Antenna 2 has only one reflection zeroes, which is observed at 5.24 GHz. Although the two antennas have the same radiator

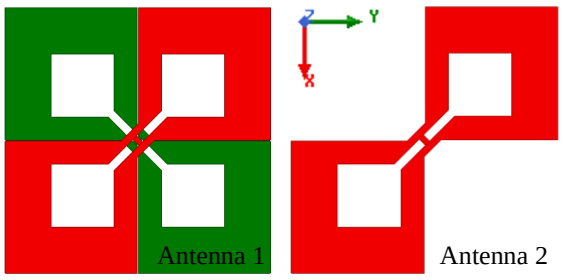

(a) (b)

Fig. 3. Simulation models of the dual-polarized antenna and single-polarized antenna. (a) Antenna 1. (b) Antenna 2.

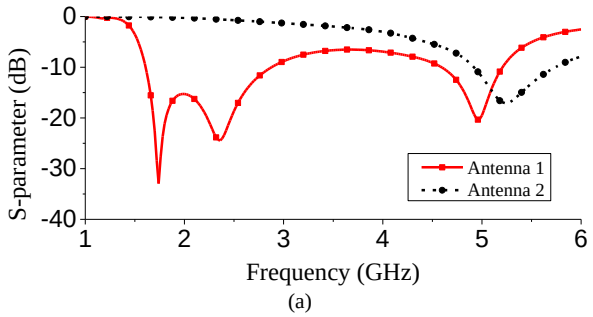

(a)

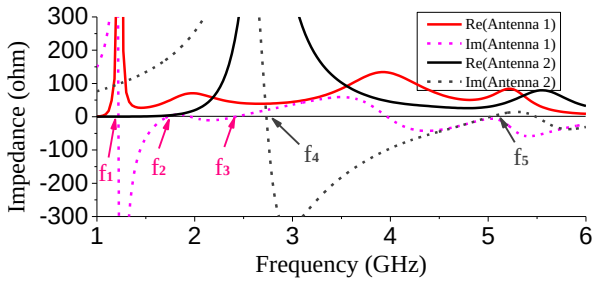

(b)

Fig. 4. Simulated results of the reference Antenna 1 and Antenna 2. (a) S-parameters. (b) Input impedances.

configuration for one polarization, different resonant frequencies are observed in the figure. With the combination of electric and magnetic resonances, the ratio of the first reflection zeroes between the Antenna 1 and Antenna 2 is about 1/3, which denotes that a significant size reduction can be achieved by using the proposed structure of Antenna 1.

To clearly illustrate the inner resonance characteristics of the two antennas, the simulated input impedances of the two antennas are shown in Fig. 4 (b). According to the definition given in [31]-[32], the natural resonance and anti-resonance can be indicated by the input impedance of the antenna. The input impedance $Z_{in}(\omega)$ of the antenna can be defined as

$$Z_{in}(\omega) = R_{in}(\omega) + jX_{in}(\omega) \quad (1)$$

where the real part $R_{in}(\omega)$ is the input resistance of the antenna, and the imaginary part $X_{in}(\omega)$ is the input reactance. If $X_{in}(\omega_0) = 0$ and $X'_{in}(\omega_0) > 0$, the frequency ω_0 is defined as the resonance frequency. Contrarily, if $X_{in}(\omega_0) = 0$ and $X'_{in}(\omega_0) < 0$, the frequency ω_0 is defined as the anti-resonance frequency.

As shown in this figure, the first anti-resonance frequency (f_4) of the single-polarized shunt loop Antenna 2 is found at 2.7 GHz with high resistance and fast variated reactance. The first

resonance frequency (f_5) is observed at around 5.1 GHz, which is the second order resonance of the shunt loop antenna, and produces a reflection zero at 5.24 GHz. Whereas the first anti-resonance frequency (f_1) of crossed shunt loop Antenna 1 is observed at 1.2 GHz, which is very lower than the first anti-resonance frequency of the single polarized Antenna 2. Two resonance (f_2 and f_3) are observed within the bandwidth at around 1.74 GHz and 2.36 GHz. Considering the values of f_1, f_2, and f_3, it can be inferred that f_3 is the second order of f_1, and f_2 is produced by the incorporation of the other pair of the crossed shunt loops. Therefore, with these two resonances, wide impedance bandwidth can be achieved for Antenna 1.

Fig. 5 shows the current distributions on the surface of the two antennas. The two reference antennas are excited for +45º polarization, and auxiliary arrows are added to help to illustrate the different resonance characteristics. As shown in Fig. 5 (a), Antenna 1 can be equivalent as a combination of two electric dipoles (in φ= 45º plane) and two magnetic dipoles (in φ= -45º plane) at the center frequency of 2.2 GHz. Two electric dipoles are of the same direction, whereas the magnetic dipoles are of the reverse direction. This can be further validated by the H-field and E-field distributions in φ= -45º plane and φ= 45º plane, respectively. As shown in Fig. 5 (c) and (d), the directions of H-field in the φ= -45º plane of the two magnetic dipoles are reverse, while the directions of the E-field in the φ= 45º plane are same.

Therefore, the resonance characteristics of the two reference antennas are totally different. Antenna 1 is a combination of electric dipoles and magnetic dipoles, and the excited shunt loops are the magnetic dipoles. However, for the excited single-polarized antenna in Fig. 5 (b), it is equivalent only as four electric dipoles and excited for +45º polarization at the first resonant frequency. Owing to the introduction of magnetic dipoles, the first impedance matching frequency moves to the much lower frequency with the dual-resonance characteristic.

Fig. 5 (e) and (f) show the current distributions of the Antenna 1 at two reflection zero frequencies of 1.74 GHz and 2.36 GHz. Two different resonances of magnetic resonance and electric resonance can be characterized. It can be seen that, when +45º polarization is excited at the first resonance of 1.74 GHz, strong current distributions are mainly distributed on the top right and bottom left loops of the antenna and form two current loops. Therefore, Antenna 1 can be equivalent as two magnetic dipoles at 1.74 GHz. While at the second resonance of 2.36 GHz, strong current distributions are mainly concentrated on the top left and bottom right loops, and flow with the same direction. So Antenna 1 can be equivalent as two electric dipoles at 2.36 GHz.

Of all the parameters for Antenna 1, the distance (d1) between the two crossed shunt loops has a more sensitive effect on the antenna impedance bandwidth, which denotes the close interaction between the electric dipoles and the magnetic dipoles. Fig. 6 shows the simulated S-parameters of Antenna 1, which varies with different length of d1. As shown in the figure, two resonances are observed within the antenna impedance bandwidth. The shorter distance will make the two resonance move together, and lower reflection coefficient within the bandwidth is achieved. Contrarily, when the value of d1 becomes bigger, two resonances will move apart, and the reflection coefficient at the center of the frequency band will be deteriorated. Therefore, the antenna impedance bandwidth can be easily controlled by this parameter.

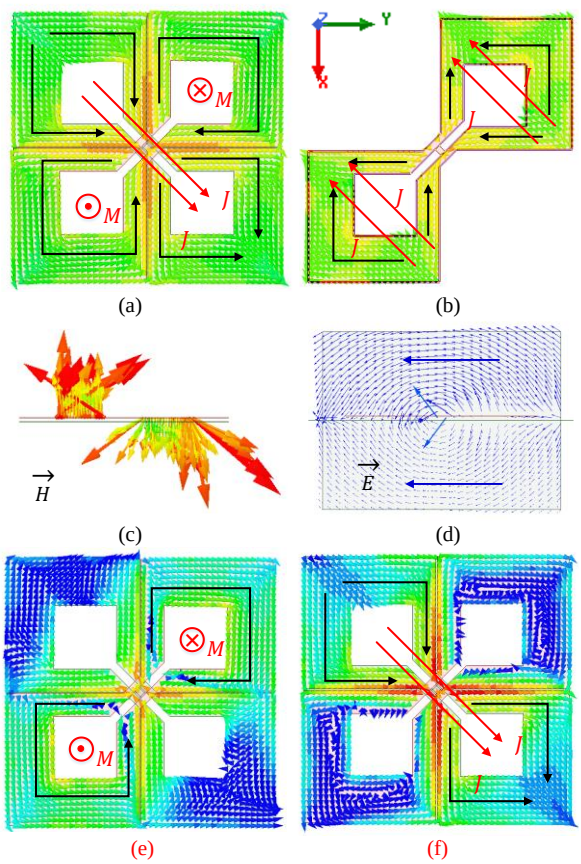

Fig. 5. Current distributions on the surface of the two antennas: (a) Antenna 1 at 2.2 GHz. (b) Antenna 2 at 5.24 GHz. H-field and E-field distributions of the reference Antenna 1 at 2.2 GHz: (c) H-field distribution in φ=-45º plane. (d) E-field distribution in φ=45º plane. (e) Current distribution of Antenna 1 at 1.74 GHz. (f) Current distribution of Antenna 1 at 2.36 GHz.

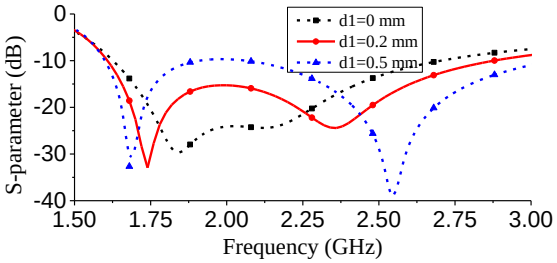

Fig. 6. Simulated S-parameters vary with different d1.

C. *Enhanced Bandwidth and Suppression*

With both the electric and magnetic resonances, wide impedance bandwidth of 1.7-2.6 GHz for S_{11} <-15 dB is achieved for Antenna 1. However, two obvious problems can be seen from Fig. 7. The first is that the impedance bandwidth is not wide enough to cover the full communication band for current 2G/3G/4G base stations. In addition, the suppression at the upper band is not very good. The simulated S_{11} from 3.4 GHz to 5 GHz is below -5 dB, and a parasitic resonance can be observed at about 5 GHz. This will bring certain interferences or blockages to the current base station systems if unwanted signals appear at these frequency bands.

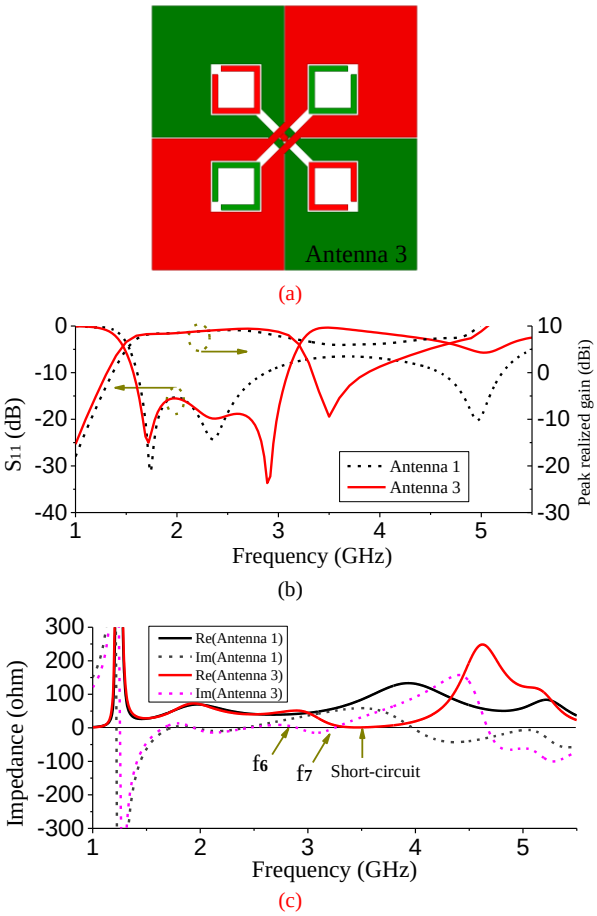

Fig. 7. Simulation model and results of reference Antenna 3. (a) Simulation model. (b) S_{11} and peak realized gain of the reference Antenna 1 and Antenna 3. (c) Input impedances of the reference Antenna 1 and Antenna 3.

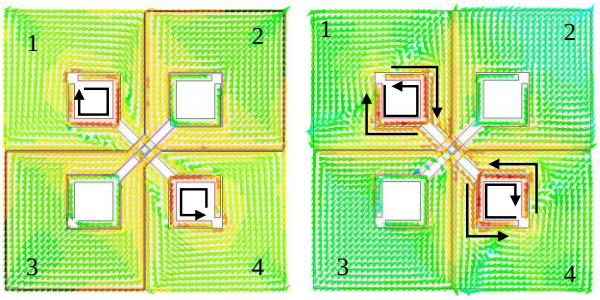

(a) (b)

Fig. 8. Current distributions on the surface of Antenna 3 at different frequencies. (a) 2.9 GHz. (b) 3.5 GHz.

To overcome these problems, four parasitic strips are introduced, and they are printed near the inner edge of the loops. The performance of the newly introduced four parasitic strips is illustrated by Antennas 3, and the simulation model is shown in Fig. 7 (a). The only difference between Antenna 3 and Antenna 1 is the introduction of the four parasitic strips. As shown in Fig. 7 (b), the first and second reflection zeroes of Antenna 3 are observed at 1.7 GHz and 2.35 GHz, which are almost the same resonant frequencies as the reference Antenna 1. However, different from Antenna 1, a third reflection zero appears at 2.9 GHz, and a steep roll-off rate is found at the upper band edge for Antenna 3. Another should be noted that a radiation null is observed at 3.5 GHz. Accordingly, a maximum reflection is

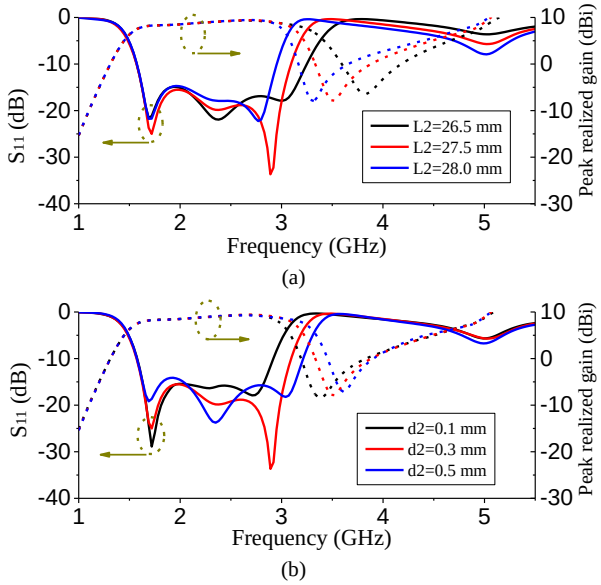

Fig. 9. Simulated S_{11} and peak realized gain of Antenna 3. (a) With different length of the parasitic strip (L2). (b) With different distance between the parasitic strip and the inner edge of the loop (d2).

also found at 3.5 GHz. The newly introduced third reflection zero at 2.9 GHz and the first suppression at 3.5 GHz can also be illustrated by the input impedances of these two antennas, as shown in Fig. 7 (c). As shown in the figure, when the parasitic strips are added into the Antenna 3, one pair of anti-resonance (f_6) and resonance (f_7) is introduced into the frequency band of interest, which produces the third reflection zero at 2.9 GHz. Moreover, very low resistance is found at 3.5 GHz with the value close to zero, which means the antenna is short-circuited at this frequency. Therefore, strong reflection is found at this frequency, and the radiation at this frequency is highly suppressed.

To further illustrate new resonance and suppression introduced by the parasitic strips, current distributions of the reference Antenna 3 at the new reflection zero at 2.9 GHz and the first suppression at 3.5 GHz are shown in Fig. 8. In Fig. 8 (a), strong current distributions are found on the surface of the two parasitic strips at 2.9 GHz. The strong current distribution on these two strips denotes that the third reflection zero is produced by the resonances of the two parasitic strips. As shown in Fig. 8 (b) at 3.5 GHz, strong current distributions are distributed not only on the surface of two strips, but also on the inner edge of the two loops. However, the current distributions on the strip and inner edge are opposite, and they cancel each other's radiation in the far field. In addition, the combination of the strip and inner edge works as a quarter wavelength open-circuited transmission line. Therefore, short-circuit is observed at the antenna input port and high suppression is achieved at 3.5 GHz.

To investigate the effect of the parasitic strips on the reflection coefficient and the realized gain for the proposed antenna, the length of the parasitic strips (L2) and the distance between the parasitic strip and the inner edge of the loop (d2) are studied. Fig. 9 (a) shows the simulated S_{11} and peak realized gain vary with the different length of the parasitic strips. It can be seen that, as the increase of the length, the third

resonance frequency shifts to the lower frequency, and the suppression frequency also moves to the lower frequency. Whereas the first and second resonant frequencies are almost unchanged with the variance of the length of the parasitic strips. This shows that the newly introduced third resonance and the first suppression have nearly no effect on the first and second resonance.

In Fig. 9 (b), as the increase of d2, the first two resonances are almost unchanged. However, with the increase of d2, the capacitance between the parasitic strip and the inner edge of the loop is decreased. Therefore, less energy is coupled from the radiating loops to the parasitic strips, which causes the third resonance and the first suppression to be shifted to higher frequencies. It should be noted that both L2 and d2 can affect the introduced resonance and suppression, but with little effect on the first two resonances. These two parameters provide much more freedom to adjust the newly introduced resonance and suppression to the desired frequencies.

D. Feed Structure

Crossed coaxial baluns are used to feed the proposed antenna with enhanced port isolation. Furthermore, a second suppression at the desired frequency of 4.9 GHz is achieved by using a shorting sheet at the end of the crossed coaxial baluns. To illustrate the working principle of the baluns, Fig. 10 compares the different feed configurations for the proposed antenna with the coaxial balun and with the unbalanced coaxial cable. Fig. 10 (a) shows the side view the proposed antenna fed by the coaxial balun. The outer conductors of the two cables are soldered to two arms of the antenna, while only one inner conductor of the cable is penetrated through one arm and soldered to the other arm of the antenna. Fig. 10 (b) shows the proposed antenna fed by ordinary unbalanced coaxial cable. The outer conductor is connected to one arm, while the inner conductor is connected to the other antenna arm.

Different impedance performances will be achieved by using two different feed structures. Fig. 11 compares the simulated S-parameters with different feed structures. In the figure, the simulated results depicted in blue colour is driven by the ideal balanced lumped port, and the simulated isolation is higher than 45 dB within the bandwidth. With the crossed baluns and the shorting sheet, the simulated isolation is better than 49 dB, which is as good as the ideal balanced lumped port driven antenna. The simulated antenna without baluns shows the worst port isolation, and the simulated isolation is only higher than 24.4 dB. Three simulated antennas show almost the same reflection coefficients within the bandwidth. Furthermore, different suppression levels are observed for the upper out-of-band. The second suppression frequency is observed at about 4.9 GHz for the proposed antenna, and the simulated reflection from 3.4 GHz to 5.4 GHz is higher than -1.7 dB. Whereas the simulated antenna without crossed baluns shows the worst suppression at around 5 GHz with two parasitic resonances. Poor suppression is also observed for the ideal lumped port driven antenna with one out-of-band parasitic resonance.

With the newly introduced shorting sheet at the end of baluns, the second suppression can be adjusted by changing the height of shorting sheet. Fig. 12 (a) shows the simulated input impedance of the antenna with and without the shorting sheet. It

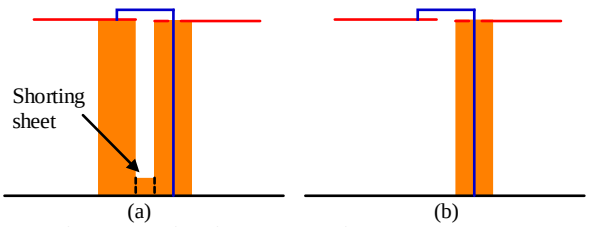

Fig. 10. Configurations of the feed structures for the proposed antenna. (a) With coaxial balun. (b) With the only coaxial cable.

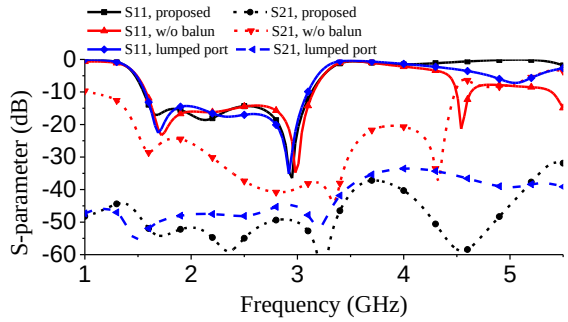

Fig. 11. Simulated S-parameters with different feed structures.

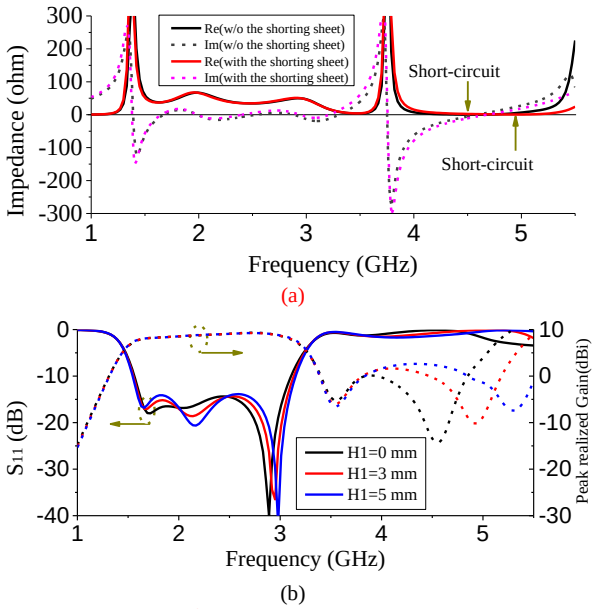

Fig. 12. Simulated results of the proposed antenna. (a) Input impedances of the proposed antenna with and without the shorting sheet. (b) S_{11} and peak realized gain with different height of the shorting sheet.

can be observed that, the shorting sheet has little effect on both the antenna input impedance within the bandwidth and the first suppression at 3.5 GHz. However, it can affect the second short-circuit frequency. As shown in the figure, when there is no shorting sheet soldered on the crossed coaxial baluns, the second short-circuit frequency with nearly zero resistance is observed at about 4.5 GHz. After the shorting sheet is introduced with the height of 3 mm, this short-circuit frequency shifts to the desired suppression frequency of 4.9 GHz. Therefore, high suppression is achieved at this frequency. To further research the working principle of the introduced suppression, the height of the shorting sheet (H1) is studied. As shown in Fig. 12 (b), with the increase of the height of the shorting sheet, the second suppression frequency moves to the

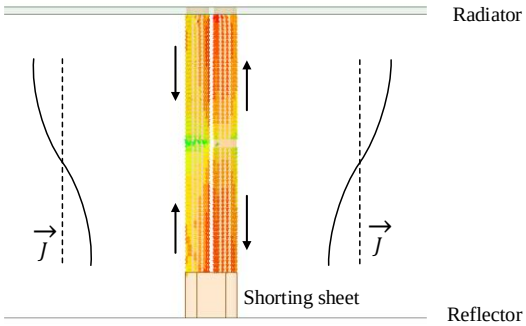

Fig. 13. Current distribution on the surface of the outer conductors for the proposed crossed coaxial baluns at 4.9 GHz.

higher frequency. Whereas the in-band impedance matching is almost unchanged. Three resonances within the band are shown with little variance, and the reflection coefficient within the bandwidth is well below -15 dB. The first suppression at 3.5 GHz is also not affected as the variance of H1. It should be noted that, H1=0 mm also denotes that the shorting sheet is not introduced to the crossed coaxial baluns. Observing from the simulated results, H1=3 mm is selected as the height of the introduced shorting sheet.

Fig. 13 shows the simulated current distribution on the surface of the crossed coaxial baluns at the second suppression frequency of 4.9 GHz when port 1 is excited, which can help to understand the principle of the second suppression. It can be seen that balanced current distribution is realized on the surface of the crossed coaxial baluns. Maximum current magnitude is observed at the position of both the antenna radiator feed point and the end of the shorting point. At the center of the balun, there is a current zero. 180 degree current phase is found at both ends of the balun, and the phases on the two coaxial cables are out-of-phase. At this frequency, the equivalent electric length of the balun is half the guided wavelength. So the feed point at the antenna radiator is short-circuited, and the input impedance will be equal to zero at 4.9 GHz. Therefore, another suppression can be achieved by adjusting the height of the shorting sheet.

III. Results and Discussion

A. Antenna Verification

To validate the antenna design concept, the proposed antenna was designed, fabricated and measured. Fig. 14 shows the photograph of the fabricated prototype of the proposed dual-polarized antenna. The antenna was measured by Anritsu 37397C vector network analyzer and ASYSOL far field antenna measurement system.

Fig. 15 compares the measured and simulated S-parameters of the proposed dual-polarized antenna. As shown in the figure, three reflection zeroes can be observed for the reflection coefficients of the two antenna ports, which agree well with the simulated reflection coefficient. The measured overlapped impedance bandwidth for S_{11}/S_{22}<-14 dB is from 1.625 GHz to 3.05 GHz (FBW=61%). In addition, maximum reflection can be seen at 3.5 GHz and 4.9 GHz. Flat upper out-of-band suppression is also observed form 3.35 GHz to 5.25 GHz, with the minimum reflection coefficient higher than -2 dB. The isolation within the bandwidth is better than 38.3 dB.

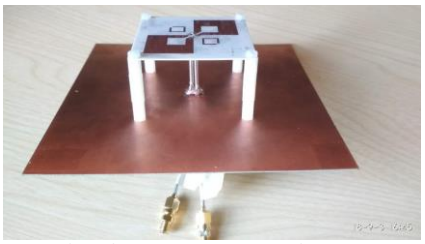

Fig. 14. Photograph of the fabricated prototype of the proposed dual-polarized antenna.

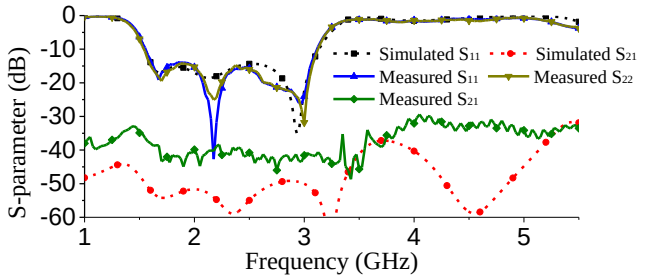

Fig. 15. Measured and simulated S-parameters of the proposed dual-polarized antenna.

Compared with the simulated isolation, due to the fabrication and assembly errors, the measured isolation is not better than the simulated isolation. However, owing to the balanced balun feed method, it is better than the reported traditional single-ended coaxial feed dual-polarized antennas.

The measured and simulated radiation patterns are shown in Fig. 16. Because of the symmetry of the proposed dual-polarized antenna, only H-plane radiation patterns excited by the antenna port 1 are given in the figure. Good agreement can be observed between the simulated and measured radiation patterns. Stable radiation patterns are also achieved within the impedance bandwidth. In addition, very low cross-polarization level can be observed in the broadside direction, which is lower than -28 dB. Owing to the antenna reflector, the measured front to back ratio of the radiation patterns is higher than 17 dB.

The measured and simulated half power beamwidth (HPBW) and peak realized gain are shown in Fig. 17. Good agreement can be observed between the simulated and measured results. The measured HPBW from 1.7 GHz to 3 GHz is 67±5°, and stable HPBW of 67±4° is achieved for the base station band. The deviation of between the simulated and the measured the HPBWs is mainly caused by the fabrication errors from the antenna radiator and reflector. Regarding the measured HPBW, it is a reasonable result for base station applications [16]. Flat antenna gain of 8.2±0.4 dBi is achieved within the impedance bandwidth. In addition, two deep antenna gain zeroes are observed at 3.5 GHz and 4.9 GHz, which are 18.1 dB and 20.6 dB lower than the maximum antenna gain, respectively.

B. Comparison

In recent years, large amounts of dual-polarized antennas are reported for base station applications. However, to the best knowledge of the authors, little of these concerns about the out-of-band suppression. As the development of 5G communication systems, this will definitely bring new inferences to the current 2G/3G/4G base station systems. Therefore, it is necessary to investigate antennas with nature suppression at 5G frequency bands for current base stations. In

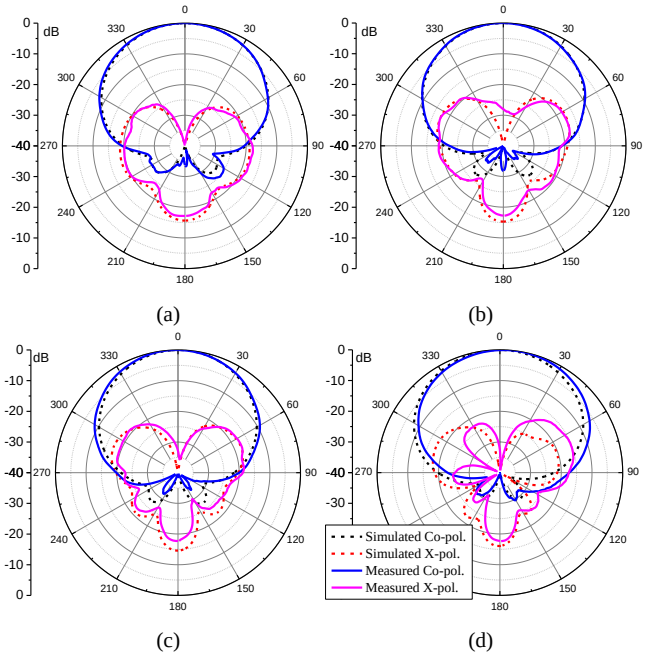

Fig. 16. Measured and simulated H-plane radiation patterns of the proposed dual-polarized antenna when port 1 is excited. (a) 1.7 GHz. (b) 2.2 GHz. (c) 2.7 GHz. (d) 3.0 GHz.

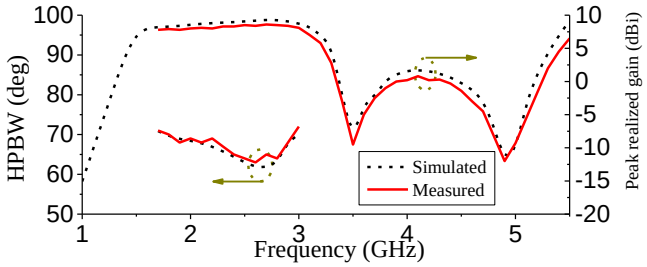

Fig. 17. Measured and simulated HPBW and peak realized gain of the proposed dual-polarized antenna when port 1 is excited.

addition, most of these reported antennas for base stations are crossed dipoles, which cover 1.7-2.7 GHz. A second-order harmonic resonance band will be normally found at about 3.4-5.4 GHz for crossed dipole antennas. Undesired harmonic radiation from 2G/3G/4G antennas will also produce interference to the 5G base station systems. Fortunately, as shown in Table I, our proposed antenna are demonstrated that two radiation nulls are achieved at 3.5 GHz and 4.9 GHz, and wide upper out-of-band suppression is realized from 3.35 GHz to 5.25 GHz with S_{11}>-2 dB.

Another feature of our proposed antenna is the compact size and high isolation. The length of the square radiator size of the recently reported antennas are around 60 mm. With the incorporation of electric resonance and magnetic resonance, smallest radiator size and widest bandwidth are achieved as compared to the reference antennas shown in the table I. In addition, by using the integrated coaxial baluns, high port isolation of 38.3 dB is also obtained for base station applications.

IV. Conclusion

This paper proposed a compact wideband dual-polarized antenna with enhanced upper out-of-band suppression. The proposed antenna is equivalent as the incorporation of electric dipoles and magnetic dipoles by using crossed shunt loops. With the combination of electric and magnetic resonances, wide impedance bandwidth and compact radiator size is achieved. Furthermore, four parasitic strips are introduced near the inner edge of loops, which makes the proposed antenna achieve the improved impedance bandwidth and obtain the first suppression at 3.5 GHz. The proposed antenna is fed by the integrated coaxial baluns with high isolation of 38.3 dB. By adding a shorting sheet to the end of baluns, the second suppression at 4.9 GHz is achieved. With the introduction of the parasitic strips and the shorting sheet, wide upper out-of-band suppression is realized from 3.35 GHz to 5.25 GHz with S_{11}>-2 dB. The proposed antenna was further fabricated and measured. Good accordance is obtained between the simulated and the measured results. With the wide bandwidth, high isolation, enhanced suppression, and stable radiation characteristic, the proposed antenna can be a good candidate for base station applications.

TABLE I
Comparison of the Dual-Polarized Antennas for Base Stations

Ref.	BW (GHz)	S_{21} (dB)	Radiator Size (mm)	Height (mm)	Suppression at 5G bands
[11]	1.69-2.5 (38.9%) RL>14 dB	-35	69	22	NG
[12]	1.7-2.2 (25.6%) RL>15 dB	-32	54	38	NG
[14]	1.66-2.75 (49.4%) RL>15 dB	-37	63	35	NG
[15]	1.68-2.74 (48%) RL>14 dB	-35	56	33	NG
[16]	1.7-2.9 (52.2%) RL>14 dB	-26	63.5	34.8	NG
[17]	1.68-2.74 (48%) RL>14 dB	-22	60	31.5	NG
This work	1.625-3.05 (61%) RL>14 dB	-38.3	47.5	33	Yes

References

[1] K. L. Wong, *Compact and Broadband Microstrip Antennas.* Hoboken, NJ, USA: Wiley, 2002

[2] L. Wen et al., "A wideband dual-polarized antenna using shorted dipoles," *IEEE Access*, vol. 6, pp. 39725-39733, 2018.

[3] S.-C. Gao, L.-W. Li, M.-S. Leong, and T.-S. Yeo, "Dual-polarized slot coupled planar antenna with side bandwidth," *IEEE Trans. Antennas Propag.*, vol. 51, no. 3, pp. 441–448, Mar. 2003.

[4] S. Gao, L. W. Li, M. S. Leong, and T. S. Yeo, "A broad-band dual-polarized microstrip patch antenna with aperture coupling," *IEEE Trans. Antennas Propag.*, vol. 51, no. 4, pp. 898–900, Apr. 2003.

[5] Y. Wang and Z. Du, "Dual-polarized slot-coupled microstrip antenna array," *IEEE Trans. Antennas Propag.*, vol. 63, no. 9, pp. 4239–4244, 2015.

[6] Y. Wang and Z. Du, "Dual-polarized dual-band microstrip antenna with similar-shaped radiation pattern," IEEE Trans. Antennas Propag., vol. 63, no. 12, pp. 5923–5928, 2015.

[7] W. Wang, J. Wang, A. Liu, and Y. Tian, "A novel broadband and high-isolation dual-polarized microstrip antenna array based on quasi substrate integrated waveguide technology," *IEEE Trans. Antennas Propag.*, vol. 66, no. 2, pp. 1–1, 2017.

[8] H. S.-M. and G. Zhang, "High-isolation, low cross-polarization, dual-polarization, hybrid feed microstrip patch array antenna for mpar application," *IEEE Trans. Antennas Propag.*, vol. 66, no. 5, pp. 2326–2332, 2018.

[9] C. Mao, S. Gao, Y. Wang, F. Qin and Q. Chu, "Multimode resonator fed dual-polarized antenna array with enhanced bandwidth and selectivity," *IEEE Trans. Antennas Propag.*, vol. 63, no. 12, pp. 5492-5499, Dec. 2015.

[10] C. Mao, S. Gao, Y. Wang, Q. Luo and Q. Chu, "A shared-aperture dual-band dual-polarized filtering-antenna-array with improved frequency response," *IEEE Trans. Antennas Propag.,* vol. 65, no. 4, pp. 1836-1844, April 2017.

[11] R. Lian, Z. Wang, Y. Yin, J. Wu and X. Song, "Design of a low-profile dual-polarized stepped slot antenna array for base station," *IEEE Antennas and Wireless Propag. Lett.*, vol. 15, pp. 362-365, 2016.

[12] Y. He, Z. Pan, X. Cheng, Y. He, J. Qiao and M. M. Tentzeris, "A novel dual-band, dual-polarized, miniaturized and low-profile base station antenna," *IEEE Trans. Antennas Propag.*, vol. 63, no. 12, pp. 5399-5408, Dec. 2015.

[13] B. Li, Y. Yin, W. Hu, Y. Ding and Y. Zhao, "Wideband dual-polarized patch antenna with low cross polarization and high isolation," *IEEE Antennas and Wireless Propag. Lett.*, vol. 11, pp. 427-430, 2012.

[14] Z. Tang, J. Liu, Y. Cai, J. Wang and Y. Yin, "A wideband differentially fed dual-polarized stacked patch antenna with tuned slot excitations," *IEEE Trans. Antennas Propag.*, vol. 66, no. 4, pp. 2055-2060, April 2018.

[15] Z. Tang, J. Liu and Y. Yin, "Enhanced cross-polarization discrimination of wideband differentially fed dual-polarized antenna via a shorting loop," *IEEE Trans. Antennas Propag.*, vol. 17, no. 8, pp. 1454-1458, Aug. 2018.

[16] D. Wen, D. Zheng and Q. Chu, "A wideband differentially fed dual-polarized antenna with stable radiation pattern for base stations," *IEEE Trans. Antennas Propag.*, vol. 65, no. 5, pp. 2248-2255, May 2017.

[17] H. Huang, Y. Liu and S. Gong, "A broadband dual-polarized base station antenna with sturdy construction," *IEEE Antennas and Wireless Propag. Lett.*, vol. 16, pp. 665-668, 2017.

[18] Y. Gou, S. Yang, J. Li and Z. Nie, "A compact dual-polarized printed dipole antenna with high isolation for wideband base station applications," *IEEE Trans. Antennas Propag.*, vol. 62, no. 8, pp. 4392-4395, Aug. 2014.

[19] J. Deng, L. Guo, Y. Yin, J. Qiu and Z. Wu, "Broadband patch antennas fed by novel tuned loop," *IEEE Trans. Antennas Propag.*, vol. 61, no. 4, pp. 2290-2293, April 2013.

[20] P. Jin and R. W. Ziolkowski, "Metamaterial-inspired, electrically small huygens sources," *IEEE Antennas and Wireless Propag. Lett.*, vol. 9, pp. 501-505, 2010.

[21] M. Tang, T. Shi and R. W. Ziolkowski, "A study of 28 ghz, planar, multilayered, electrically small, broadside radiating, huygens source antennas," *IEEE Trans. Antennas Propag.*, vol. 65, no. 12, pp. 6345-6354, Dec. 2017.

[22] M. Tang, B. Zhou and R. W. Ziolkowski, "Low-profile, electrically small, huygens source antenna with pattern-reconfigurability that covers the entire azimuthal plane," *IEEE Trans. Antennas Propag.*, vol. 65, no. 3, pp. 1063-1072, March 2017.

[23] B. Q. Wu and K. Luk, "A broadband dual-polarized magneto-electric dipole antenna with simple feeds," *IEEE Antennas and Wireless Propag. Lett.*, vol. 8, pp. 60-63, 2009.

[24] Q. Xue, S. W. Liao and J. H. Xu, "A differentially-driven dual-polarized magneto-electric dipole antenna," *IEEE Trans. Antennas Propag.*, vol. 61, no. 1, pp. 425-430, Jan. 2013.

[25] S. Zhou, Z. Peng, G. Huang and C. Sim, "Design of a novel wideband and dual-polarized magnetoelectric dipole antenna," *IEEE Trans. Antennas Propag.*, vol. 65, no. 5, pp. 2645-2649, May 2017.

[26] W. Hong et al., "Multibeam antenna technologies for 5g wireless communications," *IEEE Trans. Antennas Propag.*, vol. 65, no. 12, pp. 6231-6249, Dec. 2017.

[27] C.A. Balanis, *Antenna Theory: Analysis and Design*, John Wiley, 3rd edition, 2005.

[28] T. Tsukiji and S. Tou, "On polygonal loop antennas," *IEEE Trans. on Antennas Propag.*, vol. 28, no. 4, pp. 571-575, July 1980.

[29] S. Ahmed and W. Menzel, "A novel planar four-quad antenna," *2012 6th Europ. Conf. Antennas Propag. (EUCAP)*, Prague, 2012, pp. 1946-1949.

[30] M. A. Aprizal, A. Manda and Edwar, "Design and simulation of multi layer parasitic microstrip biquad patch antenna for WLAN 2.4GHz applications," *2017 IEEE Asia Pacific Conf. Wireless Mobile (APWiMob)*, Bandung, 2017, pp. 72-75.

[31] A. D. Yaghjian and S. R. Best, "Impedance, bandwidth, and Q of antennas," *IEEE Trans. on Antennas Propag.*, vol. 53, no. 4, pp. 1298-1324, April 2005.

[32] A. F. McKinley, T. P. White, I. S. Maksymov, and K. R. Catchpole, "The analytical basis for the resonances and anti-resonances of loop antennas and meta-material ring resonators," *J. Appl. Phys.,* vol. 112, no. 9, pp. 094911, Nov. 2012.